Chapter

Heterojunction-Based Hybrid Silicon Nanowires Solar Cell

Riam Abu Much, Prakash Natarajan, Awad Shalabny, Sumesh Sadhujan, Sherina Harilal and Muhammad Y. Bashouti

Abstract

It is known that defect-free, i.e., oxide-free, Si nanowires (Si NWs) exhibit lower defect density emissions than unmodified Si NWs. This is successfully established by grafting organic molecules on the surface. Here we show that by using a two-step chlorination/alkylation process, we are able to graft organic molecules on Si NWs for solar cell applications. Afterward, we show the electronic properties of the molecular surface (such as work function and band bending). Finally, we correlate these properties to the solar cell performance.

Keywords: silicon nanowire, defect-free surface, oxide-free silicon, chlorination/alkylation process, hybrid solar cell, oxidation resistance, photoemission, heterojunction

1. Introduction

Recently, many one-dimensional (1D) nanostructures have been realized by different methods [1, 2]. One-dimensional nanostructures such as nanowires (NWs) are considered a promising material for various applications in electronics [3], optoelectronics [4], photovoltaics [2, 5–15], and sensing [16–18].

Specifically, silicon nanowires (Si NWs) received a considerable attention since it can be integrated in the microelectronic industry. Therefore, Si NWs revealed their potential to become the mainstream building blocks of future nanodevices such as field effect transistors (FETs) [19–21] and solar cells [21–26], thus reducing process redesign costs. However, before such applications, we need at first to control the growth of the Si NWs and to understand its electronic properties. Here, we show a promising growth method and robust characterization method, i.e., the vapor-liquid-solid (VLS) method and the X-ray photoelectron spectroscopy (XPS), respectively.

Moreover, studies show that the electronic properties of Si NWs can be tuned through attachment of molecules at the surface. The high ratio between the surface and the volume of NWs makes the electronic properties highly sensitive to surface properties. To this end, grafting the surface (through dangling bonds) with organic molecules is expected to have a significant impact on the final physical and chemical properties of Si NWs. The resulting surface is known as "hybrid Si NWs" [27, 28].

However, for many applications the presence of oxide (mainly native oxide) at the Si surfaces introduces defects and decreases the device performance. Native oxide grows at the Si surface after exposure to air or/and to humidity. The defects form an undesirable layer of oxide with high impurity levels, which can result in uncontrolled

oxide/silicon interfaces. Thus, to obtain efficient Si NWs, we need to protect the surface against oxidation. For example, hydrogenated Si NWs, i.e., Si—H bonds, exhibit low surface recombination velocities [29]. However, the Si—H bonds tend to oxidize within a few minutes. Another method to functionalize the Si NW is through different bonds such as Si—C bonds, which may increase the oxidation resistance from several minutes to a few hundred hours or even months [27, 28]. Another advantage of the Si—C bonds (rather than stability and tuning the electronic properties) is their being selectively sensitive to the environment. For instance, gas sensors based on Si NWs can tune their functionality by adding special molecules at the surface with specific reactivity with the target gas [30–32]. In this article, we, first, explain how to grow the Si NWs, then how we functionalize their surface through chlorination/alkylation process, electronic properties, and finally, their application in solar cells.

2. Experimental procedure

2.1 Growth of Si NW

Si NWs were prepared by vapor-liquid-solid (VLS) method by using chemical vapor deposition (CVD) with a silane gas. The obtained Si NWs is shown in **Figure 1**.

The main steps of the VLS growth can be summarized as follows:

i. Evaporation of growth species and their diffusion and dissolution into liquid droplets

ii. Diffusion and precipitation of saturated species at the liquid—substrate interface

iii. Nucleation and growth of desired material on the interface

iv. Separation of droplets from the substrate by further precipitation and the growth of NWs

Before starting the growth, the Si substrate [the (111)] is immersed in a dilute HF solution (2%) to remove the native oxide. Subsequently, we evaporate 2 nm thick Au film or drop cast a gold nanoparticle on the Si surface. The gold nanoparticles can control the diameter of the Si NWs. The substrate is annealed

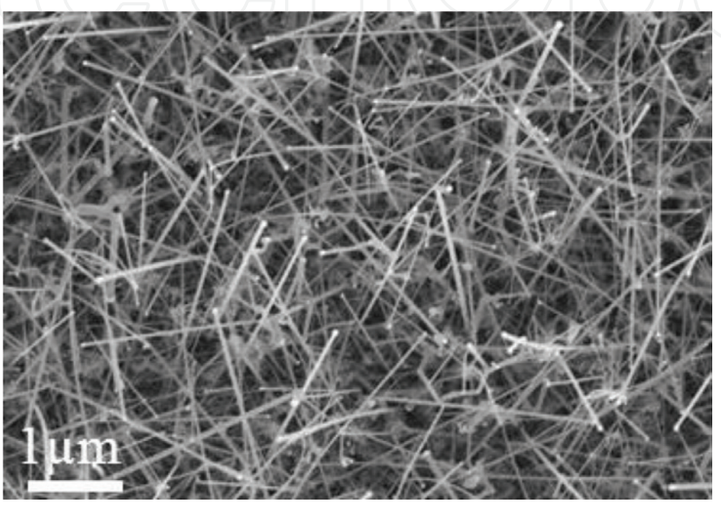

Figure 1.
SEM image of VLS-grown Si NWs with lengths of 3 ± 1 μm and diameters of 60 ± 10 nm.

Figure 2.
*The chlorination/alkylation system. In **Figure 4**, different reactions are carried in the same time.*

under vacuum at the CVD chamber to 580°C for 10 min. The temperature was then reduced to 520°C, and a mixture of 10:5 sccm (standard cm^3 min^{-1}) of Ar:SiH_4 was introduced for 20 min at a pressure of 0.5–2 mbar. The growth time can basically control the final length of the Si NWs (see **Figure 1**).

The VLS-grown Si NW can be with lengths from 1 to 20 μm and diameters of 10–100 nm [33]. As shown in the SEM image, the Si NWs were grown in random orientations.

2.2 Organic grafting via chlorination/alkylation

Among those methods developed for planar silicon, the chlorination/alkylation process is considered a promising method for molecular grafting. In this method, we cover the Si surface with Cl atoms and then convert them to R molecules. The conversion process should maintain an inert atmosphere such as reflux system or glove box (**Figure 2**).

2.3 X-ray photoelectron spectroscopy

X-ray photoelectron spectroscopy (XPS) can be used to investigate the chemical and electronic surface properties of the Si NWs. The final output of XPS measurements is the function of kinetic energy (or binding energy) versus the intensity. A schematic layout of the XPS system is depicted in **Figure 3** which shows the main components. Ay monochromatic Al K radiation (1487 eV) is irradiated to the sample to extract the core-level and valence band photoelectron spectra (0–1000 eV). They are collected at a take-off angle of 35° by a hemispherical analyzer with an adjustable overall resolution between 0.8 and 1.2 eV. In our case, it is very important to get high resolution for the following individual spectra:

i. Si 2p from 95.0 to 110.0 eV: to follow the properties of Si

ii. C 1 s from 282.0 to 287.0 eV: to figure out the grafting profile either physical or chemical grafting, molecular coverage, and functional group in the molecules

iii. 1 s from 520 to 550 eV: to follow the oxidation of the surface

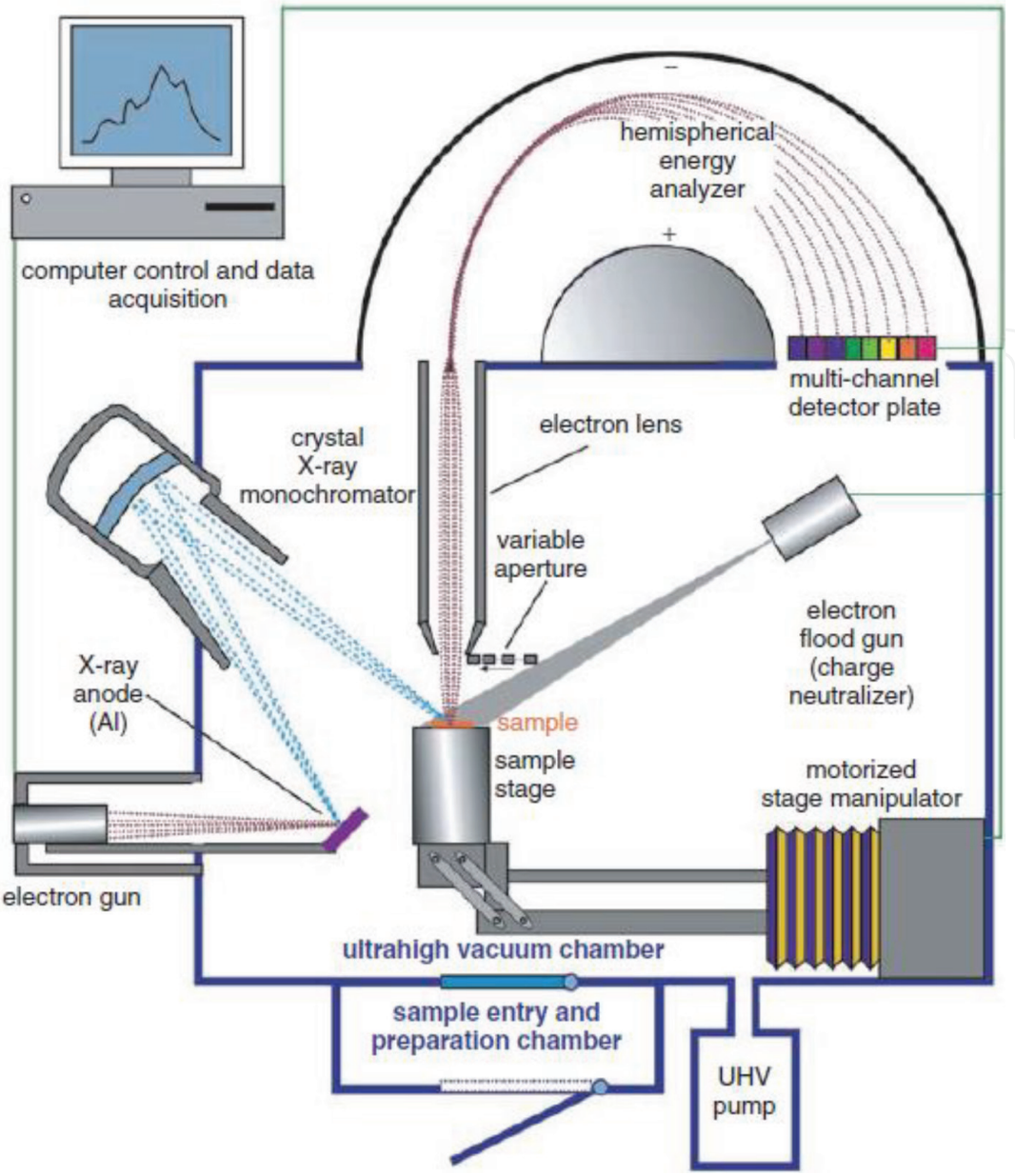

Figure 3.
Schematic layout of an X-ray photoelectron spectroscopy (XPS) system including the analyzer, sample stage, X-ray anode, X-ray monochromator, and electron gun.

The resulting XPS spectra were analyzed, and oxide levels were determined by spectral decomposition using the XPS peak software.

3. Results and discussion

Usually "hybrid materials" are used to describe two conjugated components that are chemically different. Here, we use it to define the molecular junction that are obtained after grafting an organic molecule to Si. An example for this is illustrated in **Figure 4**, where alkyl molecules are chemically attached to Si NW via Si—C bonds [27].

3.1 Organic functionalization via chlorination/alkylation

The method provides oxide-free Si and is consistent By chlorination/alkylation as shown in **Figure 5**. After hydrogenation and for the first step, we get Cl bonds by immersing the Si NWs sample in a saturated PCl_5 solution. In the second step, we

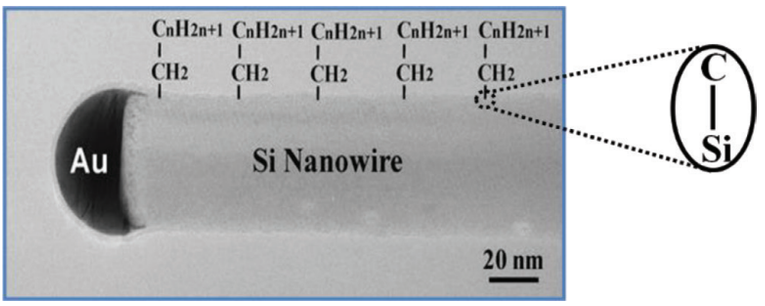

Figure 4.
Hybrid Si NW: the organic molecules (alkyl as example) are chemically connected to Si NW by covalent bonds Si—C.

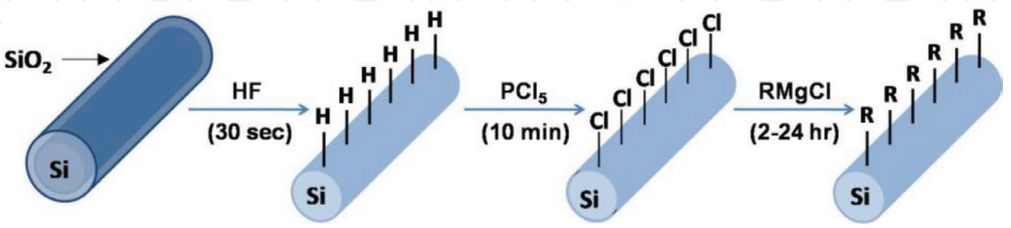

Figure 5.
Scheme illustrating the functionalization of Si NWs through the two-step chlorination/alkylation process.

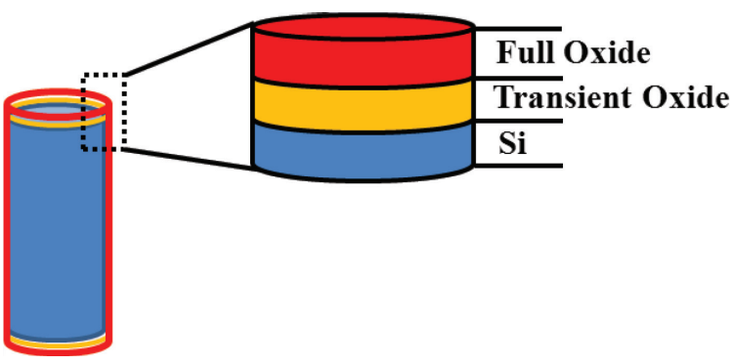

Figure 6.
Schematic diagram of SiOx/Si interface.

convert the chlorine atoms by Grignard reaction to organic molecules. The organic molecule (alkyl as an example) will be attached normally to the surface by silicon-alkyl surface bonds, i.e., Si—C bonds [30, 34].

3.2 Native oxide

The Si NWs tends to form a native oxide at the surface. The chemical stoichiometric can be explored by XPS. It was found that there are two types of Si oxide: (i) interfacial sub-stoichiometric oxides, termed as *transient oxides* including Si_2O (n = 1), SiO (n = 2), and Si_2O_3 (n = 3), and (ii) stoichiometric or full oxide SiO_2 (n = 4) as schematically shown in **Figure 6** [33–36].

3.3 Prior termination

Before any surface treatment, we removed the oxides by immersing the Si NWs in HF solution, and Si—H can be formed. Obtaining Si—H bonds has three main advantages: (i) it helps us explore oxidation mechanism since Si—H bonds are stable for a few minutes (less than 5 min), (ii) it gives full monolayer, and (iii) H-terminated is the starting step for molecular grafting [33–36].

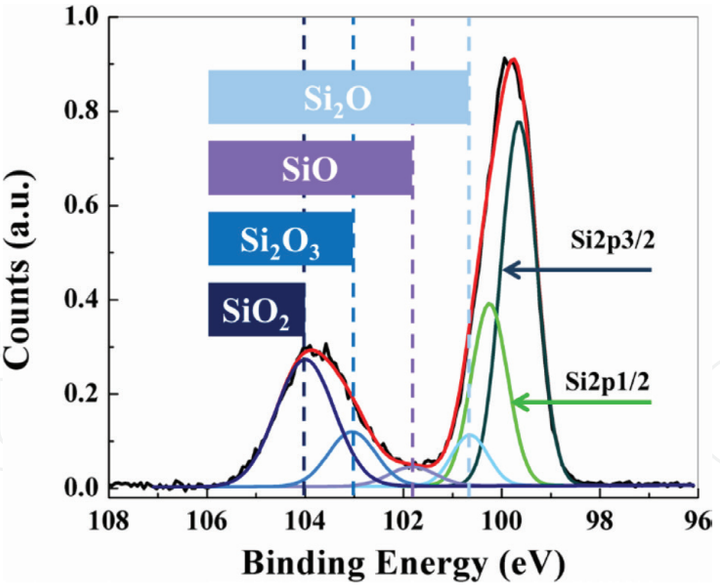

Figure 7.
XPS spectrum of Si2p core-level emission showing two silicon and four oxide peaks.

To follow the stability of the Si—H bonds or in other words to follow the oxidation of the Si NWs, we followed the Si2p emission spectra. As you can see in **Figure 7**, the Si2p emission includes two silicon spin-splitting peaks: (i) Si $2p_{1/2}$ and (ii) Si $2p_{3/2}$.

We can follow the amount of each oxide state (I_{SiOx}) by the relative integrated area under each peak. For example, we divide the integrated area under the oxide state (A_{SiOx}) by the sum of the integrated area under the Si2p, i.e., the Si$2p_{1/2}$ and Si$2p_{3/2}$ peaks ($A_{Si\ 2p1/2} + A_{Si\ 2p3/2}$). Therefore, the total oxidation (I_{ox}) can be calculated by the sum of the all the oxide states, i.e., ($I_{ox} = I_{Si2O} + I_{SiO} + I_{Si2O3} + I_{SiO2}$). It is worth to mention that the oxidation rate is different at low or high temperature (**Figure 8**). For example, Bashouti and co-authors observed different mechanisms at low temperatures (from 25 to 150°C), in which the suboxide states are the main share of the total oxide state, while at high temperatures (200–400°C), the full oxide state (i.e., SiO_2) is the main contributor to the total oxide [37, 38].

Each oxide state shows different shift and intensity relative to the Si2p. Therefore, each state has its own oxidation rate. To this end, we can calculate the respective activation energies (E_A^{ox}) of each state. Roughly speaking, since all the

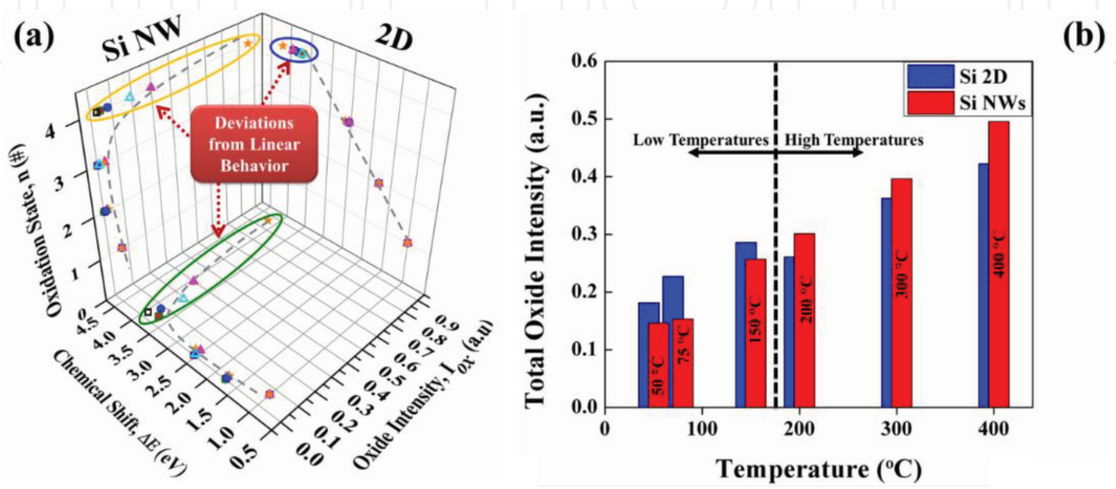

Figure 8.
(a) The sub- and full oxide distribution as function of binding energy shift and intensity per suboxide and (b) total oxide intensity of all oxide states in low and high temperature in Si NWs and 2D surfaces.

suboxides show similar rate, the E_A^{ox} was 46.35 and 23.31 meV in high and low temperature, respectively [39, 40]. The differences in the activation energies of Si NW in the high and low temperatures reveal different oxidation kinetic mechanisms:

i. **Low-temperature mechanism**: below the Si—H bonds, the back bond starts to be oxidized and turns to be suboxides. Therefore, oxidation of the backbonds (Si—O—Si) can be considered as the primary mechanism. For longer oxidation times, more backbonds are oxidized backbond form and isolated Si—OH bonds [41]. The schematic diagram of the mechanism is illustrated in **Figure 9** [42].

ii. **High-temperature mechanism**: the oxidation of the Si NWs can be attributed to the self-limited oxidation caused by the function of the initially formed oxide layer as a diffusion barrier (see **Figure 10**).

Understanding the oxidation mechanism will help us get high stable molecules on the Si NWs surface. In addition, since most of the electronic devices are operated in low temperature (below 200°C), the understanding of the low-temperature mechanism is very valuable [42].

3.4 Si2p emission

As explained above, the Si NWs show native oxide on the surface. The emission of the native oxide (without charging effect) appears in the 101–104 eV. By removing the native oxide and obtaining Si—H bonds, we can start the chlorination/alkylation process. Removing the native oxide is confirmed by the absence of the emission in 101–104 eV as seen **Figure 11** [46].

3.5 Carbon 1S emission

The emission of the C1 s confirms that the attachment via the chlorination/alkylation gives either chemical or physical bonds. Before grafting, or in the case of physical bonding, no Si—C should be available. However, in the case of chemical bond, the Si—C should be observed in the C1 s emission. For example, **Figure 12** depicts the C1 s emission of the CH_3-terminated Si NWs. Before termination, no Si—C bond was found. In this case only two emissions observed: C—C at 285.20 ± 0.02 eV and C—O at

Figure 9.
Scheme of the suggested mechanism for low-temperature oxidation of the H-terminated Si NW.

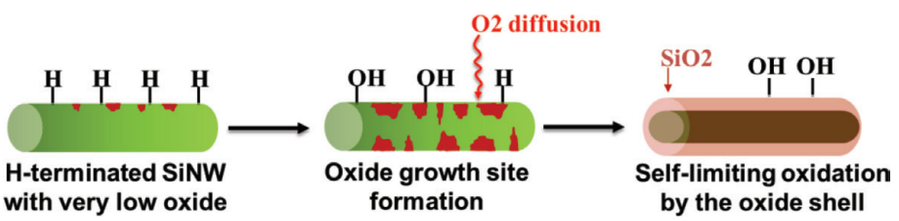

Figure 10.
Scheme of the suggested mechanism for high-temperature oxidation of the H-terminated Si NW.

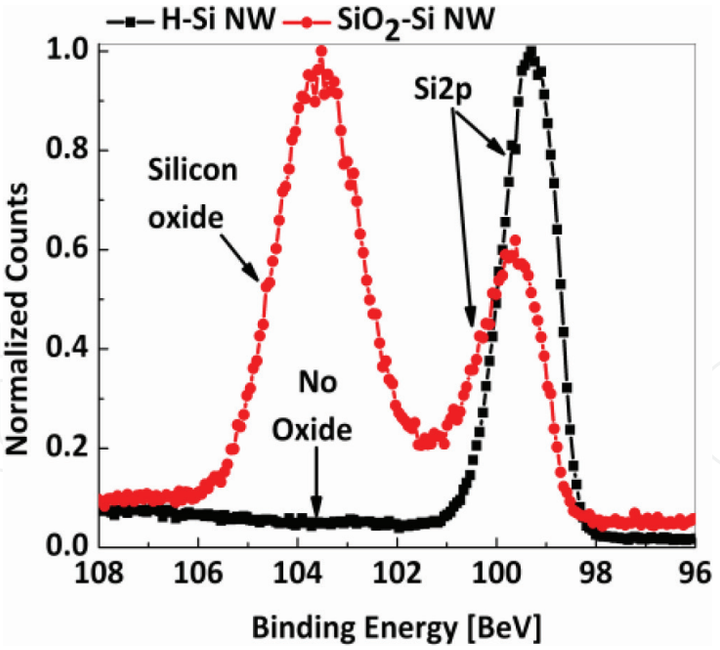

Figure 11.
Si2p emission of SiO_2—Si NW and H—Si NW.

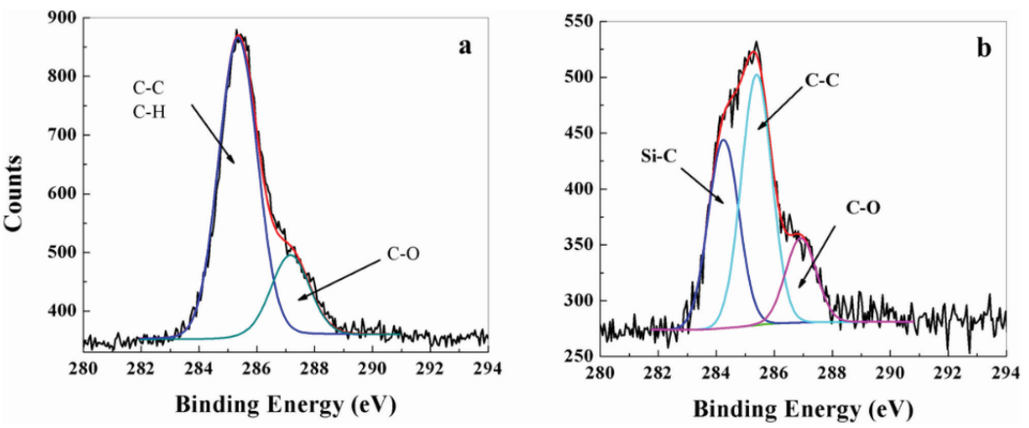

Figure 12.
XPS data from the C1 s emission region before and after alkyl-terminated Si NWs. (a) H—Si NWs show two peaks: C—C at 285.20 ± 0.02 eV and C—O at 286.69 ± 0.02 eV. (b) Methyl-Si NWs show three peaks: C—Si at 284.11 ± 0.02 eV, C—C at 285.20 ± 0.02 eV, and C—O at 286.69 ± 0.02 eV.

286.69 ± 0.02 eV which may belong to adventitious hydrocarbons. After termination, the CH_3 is chemically bonded to the Si and the Si—C is observed. Therefore, the emission of the C1 s fitted to three peaks: C—Si at 284.11 ± 0.02 eV, C—C at 285.20 ± 0.02 eV, and C—O at 286.69 ± 0.02 eV. The deconvolution method is described in [27].

3.6 Calculating the molecular density on the Si NW surface

In order to address this issue, we used a "model" molecule. In our case we chose the methyl (i.e., CH_3) since it is the smallest organic alkyl molecule with a van der Waals diameter (VDW) of 2.5 Å lower than the internuclear distance between adjacent Si atoms (3.8 Å). To this end, theoretically, the molecule should give nearly full surface density (100%), i.e., coverage (see **Figure 13**). The molecular coverage can be obtained by dividing the area under the C—Si peak to the area under the Si2p peak (sum of $Si2p_{1/2}$ and $Si2p_{3/2}$). Subsequently, we ratioed all the molecular coverage to the methyl, i.e., "$(C—Si/Si2p)_{alkyl}/(C—Si/Si2p)_{max.methyl}$" [27].

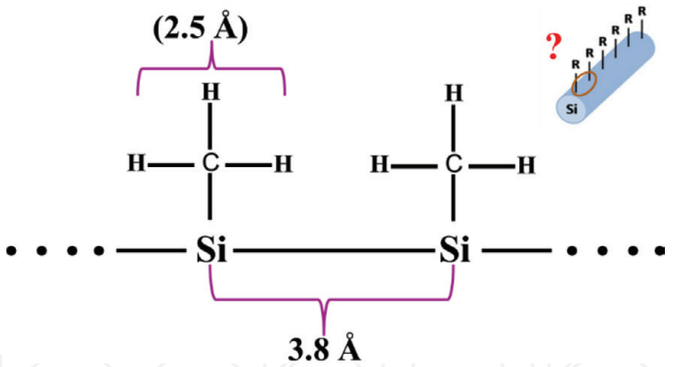

Figure 13.
Schematic diagram of methyl connected to adjacent Si atoms.

3.7 Termination of the Si NW with different molecules

Here we use alkyl molecules since they have the same structure as in methyl. The molecular coverage was found to be dependent on the steric effects which caused by the lateral interactions between the molecules. Steric effects decrease the coverage level for any molecule longer than methyl. This is due to the fact that longer molecules have higher VDW diameter (4.5–5.0 Å) than the diameter of the Si atoms. In our case, we used molecule with the form of C_nH_{2n+1} (where n = 1–10) and represented by C_n. For example, methyl and decyl are represented by C_1 and C_{10}, respectively. As the VDW diameter increases, low coverage decreases as shown in **Figure 14**.

We compare the coverage between the Si NWs and the 2D silicon. We found a similar decay but lower coverage of 10% in average than the 1Si NWs. This is maybe due to the couverture effect, which causes the molecule to be normal to the surface, and therefore, the steric effect can be lower in the case of the Si NWs. However, after > C_6, an inconsistency is observed. Based on this we can consider two main factors for grafting:

i. Molecule-substrate vertical interaction

ii. Molecule-molecule lateral interaction

The first factor can play a role in the short molecules (C_1–C_5), since they exhibit liquid-like behavior and thermal fluctuations; the determining factor is the vertical

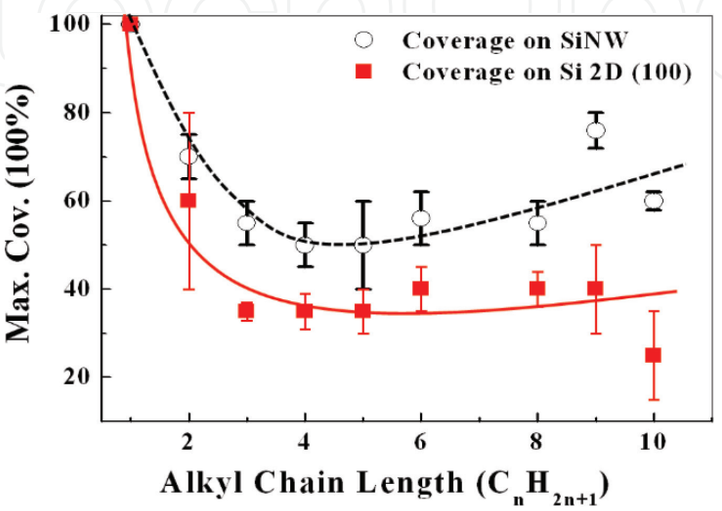

Figure 14.
Γmax-alkyl versus alkyl chain length on Si NWs and, for comparison, on 2D Si(100) surfaces. Note: (Γmax-alkyl) (C═Si/Si2p)$_{max\text{-}alkyl}$/(C═Si/Si2p)$_{max\text{-}C_1}$. Reproduced with permission from [28].

interaction [43]. The second factor may play a role in the longer molecule, i.e., (C_6–C_{10}) that forms a solid-like phase, and therefore, the lateral interactions become dominant in this regime [44].

3.8 Stability of functionalized Si NW

It was found that the stability of grafted molecules on the Si NWs is the function of several factors mainly the (i) molecular chain length, (ii) coverage level, and (iii) surface energy and diameter.

3.9 Effect of coverage and chain length

The molecular surfaces (C_1–C_{10}) were exposed to ambient air for 100 hours at room temperature, as shown in **Figure 15**. In the first days, all the alkylated Si NW show high oxide resistivity. However, after 8 days the oxide intensity became considerable and found to be dependent on the chain length and the coverage level. For example, in the case of C_3–C_6, the oxide level rose to ~0.13. However, at the same time, C_1 shows only 0.03, which is twofold higher oxidation resistance than that of C_3—C_6—Si NWs. This implies that stability of the Si NWs is dependent on the molecule coverage [28].

3.10 Effect of surface energy and diameter

Different diameters of Si NW have been used to explore the impact of the diameter: 2D (100), 2D (111), Si NW 50 nm in diameter (Si NW_{50nm}), and Si NW 25 nm in diameter (Si NW_{25nm}). To make a proper comparison, we used the same molecule (CH_3) in all the different samples. Then we exposed them to ambient air for same periods (see **Figure 16**).

Interestingly, the stability of methyl groups on Si NW is dependent on the surface. For example, the CH_3 molecule on 2D (111) was more stable than 2D (100). For example, they show the same oxidation level, but after 40 and 20 days, the Si (111) and (100), respectively, i.e., (111), show double stability than (100). The higher stability of the 2D (111) relative to the 2D (100) structure is understandable since it naturally has a 15–20% higher coverage than the 2D (100) case [45, 46].

Compering to the NWs, the NWs show almost threefold *lower* oxidation than the Si (111) and (100). These observations can be attributed to the stronger Si—C

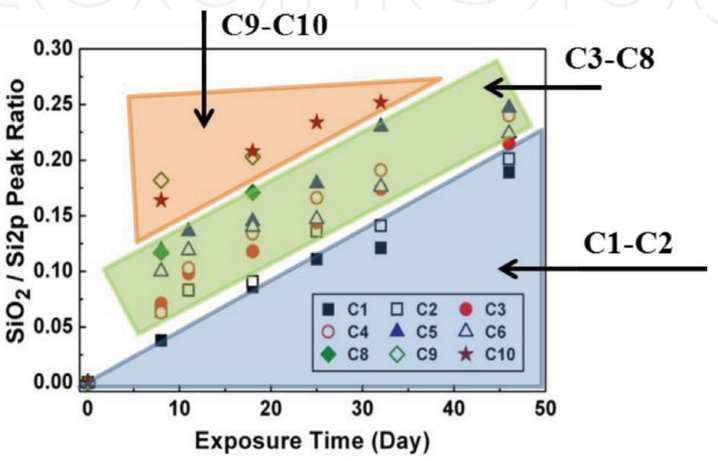

Figure 15.
Observed oxidation intensity (SiO_2/Si2p peak ratio) of alkyl-terminated Si NWs at different exposure times to ambient air. Reproduced with permission from [28].

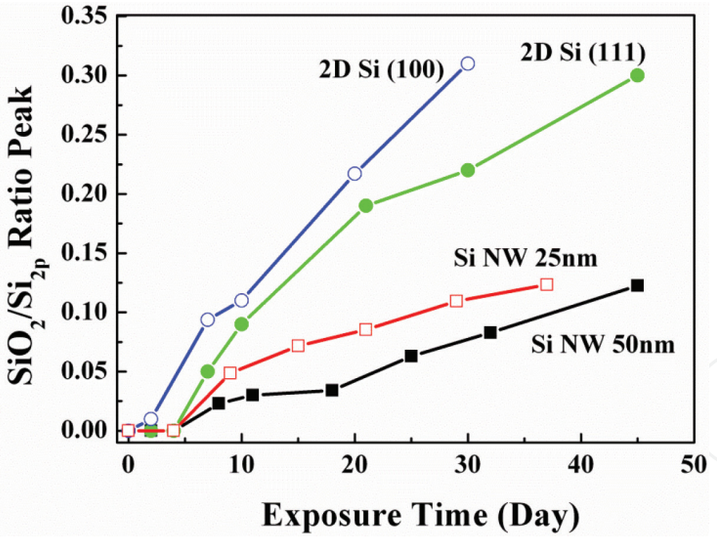

Figure 16.
Ratio of the oxidized to bulk Si2p peak areas for the methyl modification of NW_{25nm} and NW_{50nm} and 2D Si (111), exposed to air over extended time periods.

bonds on Si NW surfaces. This is supported by the shift in the Si—C bond in the NWs from 284.33 ± 0.02 eV (Si NW_{25nm}) and 284.22 ± 0.02 eV (Si NW_{50nm}) to 284.11 ± 0.02 eV for planar 2D Si. The ~0.11 ± 0.02 eV to higher binding energy ascribed to the higher reactivity of atop sites.

3.11 Effect of bonds type: π-π vs. σ-σ interactions

Not only the coverage degree and surface may affect the stability of the molecules on the Si surface. It was found that bond type interactions (π-π vs. σ-σ) can tune the stability. To check this, Si NW were embedded with methyl CH_3 and propenyl (CH_3—CH═CH— Si NWs). **Figure 17** shows the oxidation of CH_3—CH ═ CH—Si and CH_3—Si NWs. The oxidation began for the two molecules after only ~100 hours of exposure. However, after 100 hours, the propenyl shows higher stability, i.e., less oxidation. This became more clear after 180 hours; the propenyl

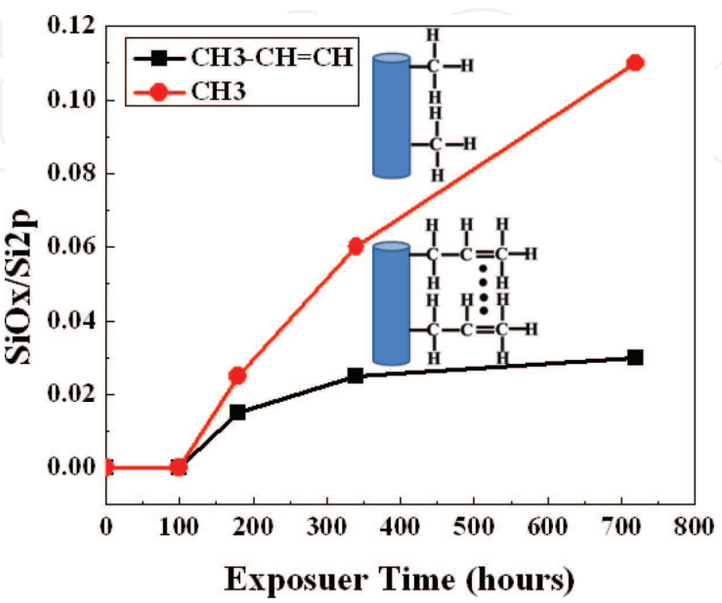

Figure 17.
Ratio of the SiO_2 to Si2p peak areas for the different surface modifications of Si NWs, exposed to air over extended time periods. Reproduced with permission from [47].

shows much lower intensity of 0.015 ± 0.005, that is, almost 8 times less than the methyl 0.11 ± 0.017. The high stability of the CH_3—CH = CH—Si NW can be attributed to the π-π interactions between the adjacent molecules [47–49].

3.12 Integration of hybrid Si NWs into solar cells

The performance of the Si solar cell can be improved by grafting molecules on the surface. Here, we present three different surface terminations: (i) H—Si NWs, (ii) SiO_2—Si NWs, and (iii) CH_3—Si NW. The surface Fermi level was calculated from the emission of the Si2p emission and the work function measured by the KP and summarized in the following table:

	H—Si NW	SiO_2—Si NW	CH_3—Si NWs
Surface Fermi level	1.05 eV	0.98 eV	0.83 eV
Work function	4.26 eV	4.32 eV	4.22 eV
Electron affinity	4.12 eV	4.29 eV	3.93 eV
Surface dipoles δ_{ss}	+0.07 eV	+0.24 eV	−0.12 eV

The electron affinity is calculated according to $\chi = \Phi - E_g + (E_F - E_V)$, while the surface dipole is calculated by χ-χ_B, when χ_B is the affinity of the bulk (4.05 eV) [50].

3.13 Photoelectron yield spectroscopy of the solar cell heterojunction

The photoemission yield (PYS) of electrons is a function of the electronic properties of the interface. As shown in **Figure 18**, each PYS shows two thresholds near 5.0 ± 0.2 and 4.2 ± 0.2 eV. The higher energy band, i.e., near the 5.0 ± 0.2, corresponds to the valence band, while the lower band 4.2 ± 0.2 eV corresponds to the defects in the band gap [50].

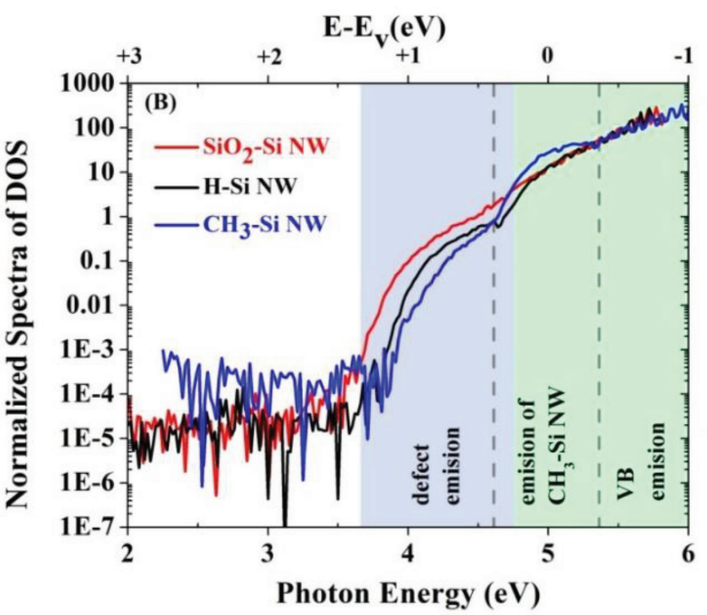

Figure 18.

Photoelectron yield Y(hν) spectral and spectral density of states of SiO_2—Si NW, H—Si NW, and CH_3—Si NW.

To compare the quality of the surface, we normalized the valence emission at 0.76 eV below the valence band maximum where they should be strongly dominated by the valence band emission only. Therefore, all the three samples show identical PYS. To this end, we can clearly see that the SiO_2—Si NWs show the highest defect density in the bandgap, while the CH_3—Si NWs show the lowest defect density.

3.14 I-V curves of solar cells

The three samples were assembled at photovoltaic cells together with polymer (PEDOT:PSS). The polymer is considered as a hole conductor, while the Si NW plays the role of light absorber and electron conductor [9]. In this cell configuration, the photo-generated electron-hole pairs are separated at a heterojunction as shown in **Figure 19**.

Four main advantages for this configuration [51, 52]:

i. Efficient light absorption

ii. Short diffusion distance of carriers

iii. Air-stable and robust polymer, PEDOT:PSS, as an efficient hole conductor [9]

iv. Utilizing only 1% of the Si used in other thin-film cells

Figure 20 shows the current-voltage (*I-V*) characteristics of CH_3—Si NW/PEDOT:PSS and SiO_2—Si NW/PEDOT:PSS solar cells under AM1.5 illumination. The SiO_2—Si NW/PEDOT:PSS shows low performance: short circuit current (J_{sc}) of 1.6 mA/cm^2, an open circuit voltage (V_{oc}) of 320 mV, a fill factor (*FF*) of 0.53, and a conversion efficiency (μ) of 0.28%. However, in the CH_3—Si NW/PEDOT:PSS, the devices show superior performance relative to the CH_3—Si NW/PEDOT:PSS and exhibit improved performance with J_{sc}, V_{oc}, *FF*, and μ magnitudes of 7.0 mA/cm^2, 399 mV, 0.44, and 1.2%, respectively.

Both samples show low values due to the high contact resistances (Rs 300 Ω). However, the comparative increase in efficiency (by about a factor of four) upon methylation proves that this kind of surface functionalization has very promising prospective.

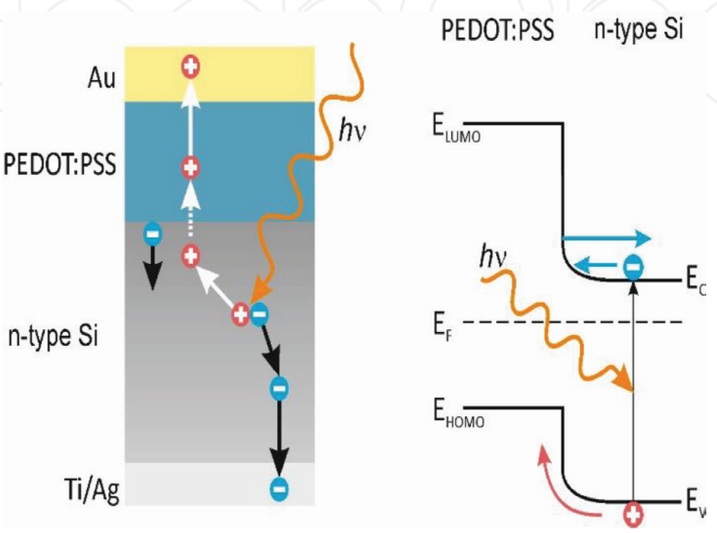

Figure 19.
Schematic diagram shows the charge separation near the Si/polymer interface.

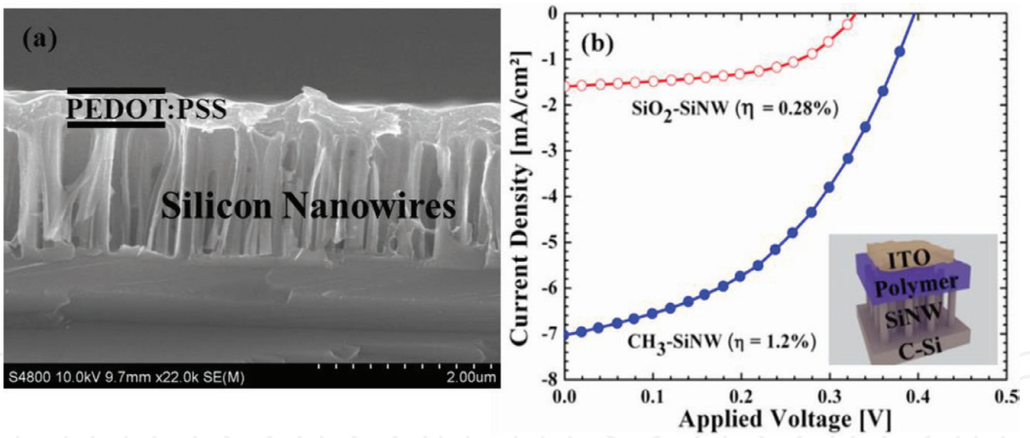

Figure 20.
(a) Tilted view of the heterojunction Si NW/PEDOT:PSS. (b) J–V characteristic under AM1.5 illuminations of the radial heterojunction solar cells from CH_3—NWs to SiO_2—NWs. Inset: schematic view of solar cell device structure.

The improved performance of the CH_3—Si NWs is attributed to the removal of the defects on the surface; therefore, the charges can transfer with low recombination rate: hole to the polymer and electron to Si. In addition, efficient charge coupling can improve the performance which will improve the charge transfer causing to an increase in V_{oc}. According to the Shockley diode equation, $V_{oc} = k_B T/q \cdot \ln(J_{sc}/J_0)$, where J_0 is the saturation current. It should be mentioned that observed gain in the V_{oc} gain cannot be explained by the increase of the current alone. Assuming a similar J_0, the increase of J_{sc} would lead to a V_{oc} gain of 0.037 V. However, we observed a gain of ΔV_{oc} = 0.079 V. This can be attributed to the grafting effect which reduces the surface recombinations (as measured by PY) and/or a favorable barrier formation (surface dipole) [50–58].

4. Conclusions

Chlorination/alkylation process was used to graft different molecules on the Si NWs. The methyl provided the highest coverage (100%) among all of the alkyl molecules (50–70%). We show different parameters that affect the stability of the molecules on the surface: molecular coverage, chain length, types of bond interactions, surface energy, and Si NW diameter. However, the propenyl (CH_3—CH═CH—Si NWs) showed excellent surface oxidation resistance: very small amount of oxides forming after more than 2 months of exposure to ambient air. Studies on the H-terminated Si NW oxidation kinetics revealed that their thermal stability relies strongly on the temperature. At lower temperatures, initially Si—Si backbond oxidation. At higher temperatures, oxygen diffusion is considered to be the initial rate-determining step, as it controls the growth site concentration.

We show that the molecules affect the solar cell performance, and a proper molecular may lead to superior solar cell performance. For instance, Si NW attached to CH_3 shows higher performance than oxide surface (by factor of four). This is attributed to the low surface recombination, low defects, and efficient charge transfer at the heterojunction. All these can be achieved by grafting a molecule of the surface. This type of heterojunction is used in advanced solar cell configurations and still under review.

Acknowledgements

This work was supported by a MAOF Grant from the Council for Higher Education in Israel for new faculty members. Dr. P. Natarajan is thankful for

the SEEDER scholarship for postdoctoral students. Awad Shalabny and Sumesh Sadhujan are appreciative of the institutional scholarships for PhD students they received from Ben-Gurion University of the Negev.

Author details

Riam Abu Much[1], Prakash Natarajan[2], Awad Shalabny[2], Sumesh Sadhujan[2], Sherina Harilal[2] and Muhammad Y. Bashouti[2,3]*

1 The Academic Arab College for Education, Haifa, Israel

2 Jacob Blaustein Institutes for Desert Research, Environmental Physics and Solar Energy, Ben-Gurion University of the Negev, Sede-Boqer, Israel

3 The IISe-Katz Institute for Nanoscale Science and Technology, Ben-Gurion University of the Negev, Beer-Sheva, Israel

*Address all correspondence to: bashouti@bgu.ac.il

References

[1] Lifshitz E, Bashouti M, Kloper V, Kigel A, Eisen MS, Berger S. Synthesis and characterization of PbSe quantum wires, multipods, quantum rods, and cubes. Nano Letters. 2003;**3**:857-862

[2] Leschkies KS, Divakar R, Basu J, Enache-Pommer E, Boercker JE, Carter CB, et al. Photosensitization of ZnO nanowires with CdSe quantum dots for photovoltaic devices. Nano Letters. 2007;**7**:1793-1798

[3] Bashouti MY, Tung RT, Haick H. Tuning the electrical properties of si nanowire field-effect transistors by molecular engineering. Small. 2009;**5**:2761-2769

[4] Schmitt SW, Schechtel F, Amkreutz D, Bashouti M, Srivastava SK, Hoffmann B, et al. Nanowire arrays in multicrystalline silicon thin films on glass: A promising material for research and applications in nanotechnology. Nano Letters. 2012;**12**:4050-4054

[5] Sivakov V, Andra G, Gawlik A, Berger A, Plentz J, Falk F, et al. Silicon nanowire-based solar cells on glass: Synthesis, optical properties, and cell parameters. Nano Letters. 2009;**9**:1549-1554

[6] Kelzenberg MD, Turner-Evans DB, Kayes BM, Filler MA, Putnam MC, Lewis NS, et al. Photovoltaic measurements in single-nanowire silicon solar cells. Nano Letters. 2008;**8**:710-714

[7] Kelzenberg MD, Turner-Evans DB, Putnam MC, Boettcher SW, Briggs RM, Baek JY, et al. High-performance Si microwire photovoltaics. Energy & Environmental Science. 2011;**4**:866-871

[8] Kim SK, Day RW, Cahoon JF, Kempa TJ, Song KD, Park HG, et al. Tuning light absorption in core/shell silicon nanowire photovoltaic devices through morphological design. Nano Letters. 2012;**12**:4971-4976

[9] Kirchmeyer S, Reuter K. Scientific importance, properties and growing applications of poly(3,4-ethylenedioxythiophene). Journal of Materials Chemistry. 2005;**15**:2077-2088

[10] Kuo CY, Gau C, Dai BT. Photovoltaic characteristics of silicon nanowire arrays synthesized by vapor-liquid-solid process. Sol Energ Mat Sol C. 2011;**95**:154-157

[11] Lee HC, Wu SC, Yang TC, Yen TJ. Efficiently harvesting sun light for silicon solar cells through advanced optical couplers and a radial p-n junction structure. Energies. 2010;**3**:784-U215

[12] Li QL, Zhu XX, Yang Y, Ioannou DE, Xiong HD, Kwon DW, et al. The large-scale integration of high-performance silicon nanowire field effect transistors. Nanotechnology. 2009;**20**:415202

[13] Lin CX, Povinelli ML. Optical absorption enhancement in silicon nanowire arrays with a large lattice constant for photovoltaic applications. Optics Express. 2009;**17**:19371-19381

[14] Liu CW, Cheng CL, Dai BT, Yang CH, Wang JY. Fabrication and photovoltaic characteristics of coaxial silicon nanowire solar cells prepared by wet chemical etching. International Journal of Photoenergy. 2012;**2012**:701809

[15] Chen C, Jia R, Yue HH, Li HF, Liu XY, Wu DQ, et al. Silicon nanowire-array-textured solar cells for photovoltaic application. Journal of Applied Physics. 2010;**108**:094318

[16] Paska Y, Haick H. Interactive effect of hysteresis and surface chemistry on gated silicon nanowire gas sensors. Acs Appl Mater Inter. 2012;**4**:2604-2617

[17] Paska Y, Stelzner T, Assad O, Tisch U, Christiansen S, Haick H. Molecular

gating of silicon nanowire field-effect transistors with nonpolar analytes. ACS Nano. 2012;**6**:335-345

[18] Paska Y, Stelzner T, Christiansen S, Haick H. Enhanced sensing of nonpolar volatile organic compounds by silicon nanowire field effect transistors. ACS Nano. 2011;**5**:5620-5626

[19] Cui Y, Zhong ZH, Wang DL, Wang WU, Lieber CM. High performance silicon nanowire field effect transistors. Nano Letters. 2003;**3**:149-152

[20] Peng KQ, Jie JS, Zhang WJ, Lee ST. Silicon nanowires for rechargeable lithium-ion battery anodes. Applied Physics Letters. 2008;**93**:033105

[21] Rurali R. Colloquium: Structural, electronic, and transport properties of silicon nanowires. Reviews of Modern Physics. 2010;**82**:427-449

[22] Haick H, Hurley PT, Hochbaum AI, Yang PD, Lewis NS. Electrical characteristics and chemical stability of non-oxidized, methyl-terminated silicon nanowires. Journal of the American Chemical Society. 2006;**128**:8990-8991

[23] Shirak O, Shtempluck O, Kotchtakov V, Bahir G, Yaish YE. High performance horizontal gate-all-around silicon nanowire field-effect transistors. Nanotechnology. 2012;**23**:395202

[24] Shu QK, Wei JQ, Wang KL, Song SA, Guo N, Jia Y, et al. Efficient energy conversion of nanotube/nanowire-based solar cells. Chemical Communications. 2010;**46**:5533-5535

[25] Eisenhawer B, Sensfuss S, Sivakov V, Pietsch M, Andra G, Falk F. Increasing the efficiency of polymer solar cells by silicon nanowires. Nanotechnology. 2011;**22**:315401

[26] Garnett EC, Yang PD. Silicon nanowire radial p-n junction solar cells. Journal of the American Chemical Society. 2008;**130**:9224

[27] Bashouti MY, Stelzner T, Berger A, Christiansen S, Haick H. Chemical passivation of silicon nanowires with C(1)-C(6) alkyl chains through covalent Si–C bonds. Journal of Physical Chemistry C. 2008;**112**:19168-19172

[28] Bashouti MY, Stelzner T, Christiansen S, Haick H. Covalent attachment of alkyl functionality to 50 nm silicon nanowires through a chlorination/alkylation process. Journal of Physical Chemistry C. 2009;**113**:14823-14828

[29] Jie JS, Zhang WJ, Peng KQ, Yuan GD, Lee CS, Lee ST. Surface-dominated transport properties of silicon nanowires. Advanced Functional Materials. 2008;**18**:3251-3257

[30] Terry J, Linford MR, Wigren C, Cao RY, Pianetta P, Chidsey CED. Determination of the bonding of alkyl monolayers to the Si(111) surface using chemical-shift, scanned-energy photoelectron diffraction. Applied Physics Letters. 1997;**71**:1056-1058

[31] Effenberger F, Gotz G, Bidlingmaier B, Wezstein M. Photoactivated preparation and patterning of self-assembled monolayers with 1-alkenes and aldehydes on silicon hydride surfaces. Angew Chem Int Edit. 1998;**37**:2462-2464

[32] Sieval AB, Linke R, Heij G, Meijer G, Zuilhof H, Sudholter EJR. Amino-terminated organic monolayers on hydrogen-terminated silicon surfaces. Langmuir. 2001;**17**:7554-7559

[33] Wagner RS, Ellis WC. Vapor-liquid-solid mechanism of single crystal growth (new method growth catalysis from impurity whisker epitaxial + large crystals Si E). Applied Physics Letters. 1964;**4**:89

[34] Bansal A, Li XL, Yi SI, Weinberg WH, Lewis NS. Spectroscopic studies of the modification of crystalline Si(111) surfaces with covalently-attached alkyl chains using a chlorination/alkylation method. The Journal of Physical Chemistry. B. 2001;**105**:10266-10277

[35] Himpsel FJ, Mcfeely FR, Talebibrahimi A, Yarmoff JA, Hollinger G. Microscopic structure of the Sio2/Si interface. Physical Review B. 1988;**38**:6084-6096

[36] Himpsel FJ, Talebibrahimi A, Yarmoff JA, Hollinger G. Microscopic structure of the Sio2/Si interface. Journal of the Electrochemical Society. 1988;**135**:C136-C136

[37] Bashouti MY, Sardashti K, Ristein J, Christiansen SH. Early stages of oxide growth in H-terminated silicon nanowires: Determination of kinetic behavior and activation energy. Physical Chemistry Chemical Physics. 2012;**14**:11877-11881

[38] Bashouti M, Sardashti K, Ristein J, Christiansen S. Kinetic study of H-terminated silicon nanowires oxidation in very first stages. Nanoscale Research Letters. 2013;**8**(1):41

[39] Whidden TK, Thanikasalam P, Rack MJ, Ferry DK. Initial oxidation of silicon(100)—a unified chemical-model for thin and thick oxide-growth rates and interfacial structure. Journal of Vacuum Science and Technology B. 1995;**13**:1618-1625

[40] Ma DDD, Lee CS, Au FCK, Tong SY, Lee ST. Small-diameter silicon nanowire surfaces. Science. 2003;**299**:1874-1877

[41] Mawhinney DB, Glass JA, Yates JT. FTIR study of the oxidation of porous silicon. The Journal of Physical Chemistry. B. 1997;**101**:1202-1206

[42] Tian RH, Seitz O, Li M, Hu WC, Chabal YJ, Gao JM. Infrared characterization of interfacial Si–O bond formation on silanized flat SiO2/Si surfaces. Langmuir. 2010;**26**:4563-4566

[43] Schwartz DK. Mechanisms and kinetics of self-assembled monolayer formation. Annual Review of Physical Chemistry. 2001;**52**:107-137

[44] Nuzzo RG, Zegarski BR, Dubois LH. Fundamental-studies of the chemisorption of organosulfur compounds on Au(111)—implications for molecular self-assembly on gold surfaces. Journal of the American Chemical Society. 1987;**109**:733-740

[45] Sivakov VA, Scholz R, Syrowatka F, Falk F, Gosele U, Christiansen SH. Silicon nanowire oxidation: The influence of sidewall structure and gold distribution. Nanotechnology. 2009;**20**:405607

[46] Bashouti MY, Paska Y, Puniredd SR, Stelzner T, Christiansen S, Haick H. Silicon nanowires terminated with methyl functionalities exhibit stronger Si–C bonds than equivalent 2D surfaces. Physical Chemistry Chemical Physics. 2009;**11**:3845-3848

[47] Assad O, Puniredd SR, Stelzner T, Christiansen S, Haick H. Stable Scaffolds for reacting Si nanowires with further organic functionalities while preserving Si–C passivation of surface sites. Journal of the American Chemical Society. 2008;**130**:17670

[48] Puniredd SR, Assad O, Haick H. Highly stable organic monolayers for reacting silicon with further functionalities: The effect of the C–C bond nearest the silicon surface. Journal of the American Chemical Society. 2008;**130**:13727-13734

[49] Puniredd SR, Assad O, Stelzner T, Christiansen S, Haick H. Catalyst-free functionalization for versatile modification of nonoxidized silicon structures. Langmuir. 2011;**27**:4764-4771

[50] Bashouti MY, Pietsch M, Brönstrup G, Sivakov V, Ristein J, Christiansen S. Hybrid polymer/silicon nanowire solar cell with high efficiency through covalent Si–C terminated surface passivation. Prog. Photovolt: Res. Appl. 2014;**2**:1050-1061

[51] Putnam MC, Boettcher SW, Kelzenberg MD, Turner-Evans DB, Spurgeon JM, Warren EL, et al. Si microwire-array solar cells. Energy & Environmental Science. 2010;**3**:1037-1041

[52] Tian BZ, Zheng XL, Kempa TJ, Fang Y, Yu NF, Yu GH, et al. Coaxial silicon nanowires as solar cells and nanoelectronic power sources. Nature. 2007;**449**:885-U888

[53] Maldonado S, Knapp D, Lewis NS. Near-ideal photodiodes from sintered gold nanoparticle films on methyl-terminated Si(111) surfaces. Journal of the American Chemical Society. 2008;**130**:3300

[54] Ambrico M, Ambrico PF, di Mundo R. Electrical transport Features of SiNWs random network on Si support after covalent attachment of new organic functionalities. Nanomater. Nanotechnol. 2012;**2**:1-8

[55] Zhong Y, Xiao Y, Chen Q, Zhu H. Heterojunction solar cells based on graphene woven fabrics and silicon. Materiomics. 2018;**4**:135-138

[56] Yu L, Tune D, Shearer C, Grace T, Shapter J. Heterojunction solar cells based on silicon and composite films of polyaniline and carbon nanotubes. IEEE J. Photo Volt. 2016;**6**

[57] Silicon Based Heterojunction Solar Cells and Photodetectors. Ph.D. thesis Zhen Gao

[58] Ghosh BK, Weoi CNJ, Islam A, Ghoshb SK. Recent progress in Si hetero-junction solar cell: A comprehensive review. Renewable and Sustainable Energy Reviews. 2018;**82**:1990-2004